Homopolymeric Protein Phosphors: Overpassing the Stability Frontier of Deep-Red Bio-Hybrid Light-Emitting Diodes

*Sara Ferrara, Juan P. Fernandéz-Blázquez, Juan Pablo Fuenzalida Werner, and Rubén D. Costa**

Although protein-polymer phosphors are an emerging photon-management filter concept for hybrid light-emitting diodes, deep-red-emitting devices based on archetypal fluorescent proteins (FPs; mCherry) are still poorly performing with lifetimes <50 h under high photon-flux excitation and ambient conditions. Here, the challenge is two-fold: i) understanding the deactivation mechanism of red-emitting FP-polymer coatings and, in turn, ii) identifying the best polymer design for highly stable devices. This study first provides comprehensive photophysical/thermal/structural studies and device degradation (ambient/inert) analysis, revealing the presence of photo-induced *cis–trans* isomerization and the effect of oxygen and water on the deactivation of mCherry in reference polymer coatings. Based on these findings, a new bio-phosphor configuration using polyvinyl alcohol derivatives, in which crystallinity and amount of trapped water (stiffness and oxygen/moisture barriers) are easily controlled by the hydroxylation degree, is successfully achieved. Compared to the prior art, these devices significantly outperform the reference stability (>50-fold enhancement), showing a brightness loss of <5% over the first 2000 h and a final device lifetime of 2600 h. Hence, this study describes a unique rationale toward designing polymers to stabilize FPs for lighting, overpassing stability frontiers in deep-red hybrid light-emitting diodes (HLEDs) going from hours to months.

1. Introduction

In the quest for highly performing artificial lighting sources, inorganic light-emitting diodes (LEDs) stand out.[1–3] However,

S. Ferrara, J. P. Fuenzalida Werner, R. D. Costa
Technical University of Munich
Chair of Biogenic Functional Materials
Schulgasse 22, 94315 Straubing, Germany
E-mail: ruben.costa@tum.de
J. P. Fernandéz-Blázquez
IMDEA Materials Institute
Calle Eric Kandel 2, 28906 Getafe, Spain

The ORCID identification number(s) for the author(s) of this article can be found under https://doi.org/10.1002/adfm.202300350.

sustainability and health issues are related to the use of inorganic phosphors (IPs) that i) are based on either rare-earth or toxic photon down-converting emitters,[4] ii) leave a strong blue component responsible for alteration of the circadian rhythm and damage at the eye photoreceptors,[5] and iii) are not efficiently recycled to date.[6] Thus, IPs are considered as the major concern toward the next generation of the artificial lighting based on the LED technology.[7]

In this scenario, hybrid LEDs (HLEDs) aim at replacing IPs with organic photon down-converting filters or organic phosphors (OPs).[8] They have traditionally combined organic emitters e.g., small molecules, coordination complexes, polymers, carbon dots with polymers, MOFs, etc. as packaging matrices, reaching average stabilities of around a few days at luminous efficiencies < 50 lm W^{-1}.[9–12] Though this field began at the end of the '90s,[13,14] recent advances have set in their relevance. Among them, bio-phosphors implementing biogenic components[15] have recently emerged as a new family with best stabilities for green-emitting devices over thousands of hours at luminous efficiencies > 100 lm W^{-1}.[16] Here, three families have been reported. At first, artificial emitters embedded in bio-derived matrices, such as DNA,[17] proteins,[18] polysaccharides,[19,20] and cellulose,[21] have reached maximum luminous efficiencies of ≈35 lm W^{-1}. In 2016 natural fluorescent proteins (FPs) were stabilized in polymer coatings, resulting in devices baptized as Bio-HLEDs with a loss of emission intensity < 10% (50 lm W^{-1}) after 100 h of continuous operation at low power.[15] Enhancing the polymer-FP interface led to green-emitting Bio-HLEDs with stabilities > 150 d at luminous efficiencies of ≈130 lm W^{-1}.[16] Several groups have further developed Bio-HLEDs employing both natural[16,22–26] and artificial FPs.[27,28] Finally, fully FP-based biogenic phosphors, in which both the packaging matrix and the emitter are of biological origin have been recently reported, e.g., silk fibroin (SF).[29]

The challenge in Bio-HLEDs based on natural FPs is twofold. On one hand, preserving the bio-functionality of FPs upon preparing thin films requires the use of a suitable polymer mixture that must feature i) a good compatibility with FPs in

aqueous media, ii) good mechanical properties to enclose FPs in a stiff environment, iii) easy preparation and processability in self-standing films with arbitrary thickness and shapes, and iv) efficient recyclability. To date, the strategy has been a composite composition, in which a small and branched polyethylene oxide was used to shield FPs, and large and linear polymers were mixed to control rheological and/or mechanical features of the final FP-polymer composite.[15,16] The major limitation is the phase separation, that reduces FP stability and optical features, e.g., undesired scattering effects and/or opacity. On the other hand, the performance of Bio-HLEDs based on red-emitting FPs is still poor (< 50 h) compared to the green-emitting FP counterparts (< 3,500 h), representing a critical bottleneck toward highly performing white Bio-HLEDs.[22,30] Here, the archetypal red-emitting FP has been mCherry, which is a monomeric β-barrel protein structure embedding a DsRed-like chromophore.[31,32] This FP features a narrow emission centered at 620 nm with photoluminescence quantum yields (ϕ) of *ca.* 20%, leading to Bio-HLEDs with stabilities < 50 h using reference polymer composites.[15,23] Thus, the optimized protocol to prepare highly emissive and stable red-emitting FP-polymer filters based on a comprehensive study about their degradation mechanism under device operation conditions is critical to realize white protein-based lighting devices.

This work first rationalizes the degradation mechanism of mCherry in a traditional polymer composite with respect to the H-transfer mediated *cis-trans* isomerization and the role of water-/oxygen-assisted processes. With this information at hand, a new homopolymeric matrix based on the hydrophilic polyvinyl alcohol (PVA) was studied to successfully stabilize mCherry in homopolymeric coatings. In short, a series of PVA derivatives controlling the effect of the hydroxylation grade was studied to regulate trapped water content and crystallinity grade that are key toward first-class red-emitting Bio-HLEDs. As the most remarkable performance, mCherry-PVA on-chip devices featured stabilities spanning from 1100–2,600 h under ambient and continuous irradiation, representing 1–2 orders of magnitude enhancement compared to the prior art (< 50 h).[15,23] Hence, this work sets in a solid step-stone in deep-red Bio-HLEDs, providing crucial information to i) understand the photo-induced degradation mechanism of mCherry in reference polymer composites depending on the environmental conditions, i) simplify the stabilization of FPs using homopolymeric filters, and iii) develop record stable red-emitting Bio-HLEDs, making realistic the progress toward white-emitting protein-based lighting.

2. Results and Discussion

2.1. Preparation and Characterization of Reference mCherry-Polymer Bio-Phosphors

Bio-phosphors were prepared by embedding 1 mg of mCherry in reference TMPE:PEO composite matrix with a 4:1 mass ratio following the procedure reported elsewhere (5 mm diameter and 2 mm height – **Figure 1**) see Experimental Section.[15] In detail, the mCherryTMPE aqueous solutions were prepared with either milli-Q water (6% PBS, sample **a**) or D$_2$O (6% PBS,

sample **b**). Linear PEO was added under gentle stirring conditions and the mixture was immediately dried at 3 mbar.

Figure 1 and **Table 1** summarize the photoluminescence features of the above bio-phosphors. In short, they consist of i) an intense fluorescence band centered at ≈640 nm with excited-state lifetimes (τ) of 1.5–9 ns and ϕ of *ca.* 20% and ii) an excitation spectra with three well-defined bands ascribed to the protein chromophore (450–600 and 320–430 nm) and the presence of the aromatic tryptophan amino acids (< 300 nm). In both cases, the lack of a well-defined vibrational structure for both, the emission and the excitation spectra, suggests a certain degree of agglomeration upon coating preparation – Figure S1 (Supporting Information). This leads to slightly different τ values (Table 1) and a ca. 30 nm red-shifted emission maxima wavelength compared to that in solution (610 nm; Table 1), that could be related to structural distortions of the β-barrel and/or the H-chain distribution, slightly changing i) the chromophore conformation,[33] ii) the protonation degree of its imidazolinone moiety in the ground state,[31,33] and/or iii) the H-bonding network interacting with the acylimine oxygen in the excited state.[34] Finally, a very low intense emission at 420 nm points out the presence of no fully maturated proteins bearing the TagBFP-like form of the chromophore.[33] According to this mechanism, the first steps involve the tripeptide cyclization to form the N-acylimine and successive dehydration and oxidation at the level of the imidazolinone moiety (steps 1→2→3 in Figure 1). Next, an oxidation of the Cα−Cβ bond of Tyr chromophore leads to the final DsRed product (step 3→4 in Figure 1). This means that the proper evolution of the chromophore from its blue to the red form requires several stages of dehydration and, most importantly, oxidation.

Deep-red Bio-HLEDs were then prepared by combining **a** and **b** coatings with a 590 nm LED chip using on-chip configuration i.e., the phosphor is placed directly on top of the pumping chip. These devices were driven at 200 mA (55 mW cm^{-2}) under ambient (25 °C and 45% moisture; **a-a** and **b-a** devices) and inert (N$_2$, 25 °C, and < 0.1 ppm H$_2$O/O$_2$; **a-i** and **b-i** devices) atmospheres, monitoring both temperature and emission intensity of the mCherry coatings. While the temperature of the bio-phosphors held 25–30 °C regardless of the type of sample and conditions, the emission intensity decay profile was different. In short, **a-a** and **b-a** devices exhibited a three-stage intensity decay mechanism, while **a-i** and **b-i** devices showed a two-stage deactivation – Figure 1. All the devices showed a first stage characterized by *ca.* 30–40% intensity loss over the first 2 h. This has been attributed to i) the degradation of monomeric and/or aggregate-like FPs that are not well-stabilized in the polymer matrix i.e., reduction of the intensity ratio between chromophore and tryptophan emission intensity; I$_c$/I$_{tr}$, ii) temperature induced conformation changes of the FP-polymer interface, and iii) thermal emission quenching as the coating temperature raised.[29] While the latter must not play a major role as the temperature rise is of maximum 5 °C, a close inspection of the emission features at both, UV and visible regions – Figure 1, points out that the emission spectra undergo a progressive blue-shift of the maximum emission wavelength of the chromophore (*ca.* 5–10 nm) associated to a reduction of τ values and unchanged ϕ values – Table 1, as well as the appearance of a new tryptophan emission band centered

**ADVANCED
SCIENCE NEWS**

www.advancedsciencenews.com

**ADVANCED
FUNCTIONAL
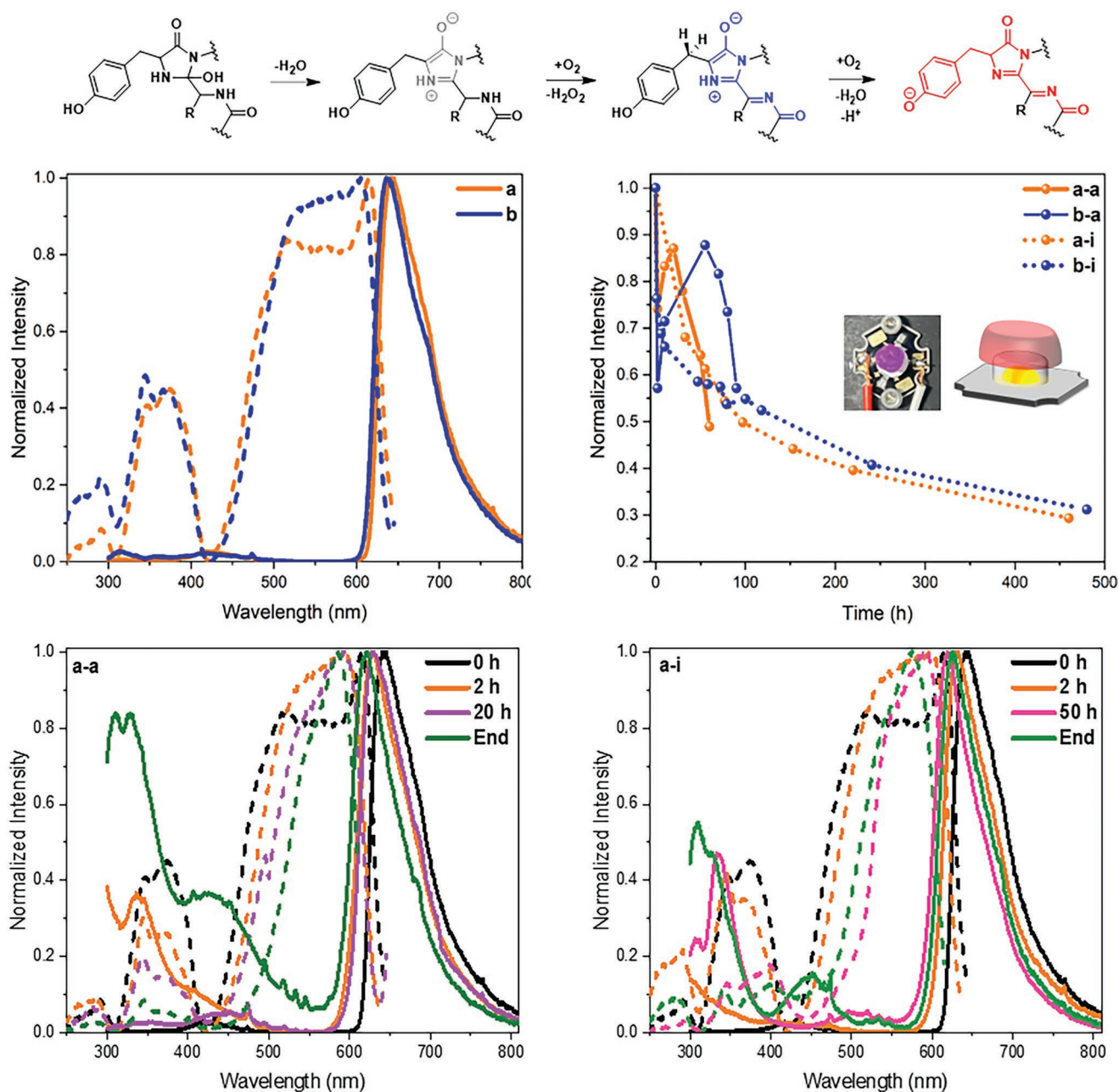MATERIALS**

www.afm-journal.de

Figure 1. Top: Formation of the DsRed chromophore via TagBFP-like chromophore mechanism. The N-acylimine is formed by the tripeptide cyclization followed by dehydration/oxidation steps (steps 1→2→3). Step 3→4 is the oxidation of the Cα–Cβ bond of Tyr chromophore.[33] Middle: Emission (solid line; λ_{exc} = 280 nm) and excitation (dashed line; λ_{em} = 680 nm) spectra of mCherry-TMPE:PEO bio-phosphors (left) and emission intensity decay profile (λ_{em} = 685 nm) of mCherry-TMPE:PEO devices under 590 nm irradiation at 55 mW cm^{-2}, on chip (right); inset: sketch of an operating device with a 590 nm LED chip as a pumping source on the bottom, with a red emitting phosphor placed directly on chip and real mCherry TMPE:PEO coating on top of the LED source. Bottom: Emission (solid line; λ_{exc} = 280 nm) and excitation (dashed line; λ_{em} = 680 nm) spectra of the mQ mCherry-TMPE:PEO bio-phosphors at each degradation stage of the devices (see legend) operating at under ambient (left) and inert (right) atmospheres. All the phosphors irradiated upon both ambient and inert conditions showed constant temperature <30 °C.

at *ca.* 330 nm. In contrast to GFP-like proteins, mFruits-like proteins typically experience several photo-induced processes: i) blue-shifted emission has been attributed to changes of the deprotonation of Glu 215, modifying H-chain around the imidazolinone moiety of the chromophore,[31] ii) reduction of the ϕ values related to the less coplanarity of the chromophore structure and/or rigidification of the chromophore,[31,35–37] and

iii) prominent isomerization from *cis* (emissive native form) to *trans* (dark state).[38,39] Thus, the first stage should combine i) a quick *cis* to *trans* isomerization under strong photon flux saturation[38] that is allowed by the increase of the chromophore cavity volume upon distortion of the β-barrel structure vide supra, and ii) a slow deprotonation of the Glu 215 leading to blue-shifted emission spectra.

Table 1. Photophysical features of mCherry solutions in mQ and D_2O water, as well as fresh and irradiated reference mCherry-polymer mQ- and D_2O-based bio-phosphors (**a**, **b**) upon ambient/inert (a/i) conditions.

	λ_{exc} [nm]	λ_{em} [nm]	ϕ [%]	τ [ns]	k_r [a] $[s^{-1}]$	k_{nr} [b] $[s^{-1}]$	I_c/I_{tr}
mCherry Milli-Q	585	610	20.0	1.57	1.27	5.10	/
mCherry D_2O	585	610	26.1	2.22	1.17	3.33	/
a	610	642	23.1	1.51	1.52	5.10	/
b	605	638	23.0	1.78	1.29	4.33	/
a-a/i 2 h	590/590	630/630	18.1/21.3	1.35/1.43	1.43/1.68	6.45/6.20	50/8
a-a/i 20 h	590/590	630/625	18.1/23.5	1.27/1.43	1.19/1.64	5.39/5.35	¾
a-a/i 100 h	585/575	622/620	16.1/16.5	1.52/1.53	1.13/1.08	5.87/5.46	1.2/2
b-a/i 2 h	595/605	625/630	25.2/18.3	1.43/1.64	1.79/1.12	5.30/4.98	6/16.6
b-a/i 50 h	585/580	620/620	16.1/23.0	1.41/1.50	1.19/1.53	6.21/5.13	3/7.7
b-a/i 100 h	585/580	620/615	9.32/20.8	1.35/1.60	0.69/1.30	6.72/4.95	0.6/0.5

[a,b] $\times 10^8$.

Much more striking, **a-a** and **b-a** devices showed a second stage characterized by an emission intensity recovery that almost reaches the initial intensity i.e., 10% loss remains. This process requires 20 h a) and 50 h b), suggesting that an H-transfer mechanism must be involved as the presence of D_2O typically slows down the process rate associated with these phenomena in FP aqueous solutions i.e., isotopic effect.[40] In stark contrast, this increase is not present in **a-i** and **b-i** devices, in which a further very slow intensity decay is noted. Thus, exchange of oxygen with the surrounding is instrumental in this recovery. Indeed, the TMPE:PEO matrix exhibits a high permeability to oxygen and a gel-like texture that does not provide a stiff environment.[15,16,23] Further insights are revealed by the analysis of the photoluminescence features in Figure 1. At first, the emission band shape of the chromophore kept a progressive blue shift (*ca.* 20 nm) and the τ values are further reduced regardless of the atmosphere conditions Table 1, suggesting that the Glu 215 deprotonation process is still active. Second, the ϕ values hold constant in Table 1, indicating that the degree of co-planarity and/or chromophore packing is not meaningfully affected. Third, the tryptophan emission intensity increases, indicating that the chromophore still transforms to a non-emissive form. In previous studies concerning the mCherry chromophore transformation,[33] the processes that could explain the intensity increase under ambient conditions could be either i) the change in the concentration of long-lived dark mCherry states[38] that should be independent of ambient oxygen or ii) the final maturation step from TagBFP-like chromophore to its red-emitting form involving an oxidation and H-transfer, as previously described and illustrated in Figure 1.[41,42] As indicated in the emission spectrum of the fresh coating in Figure 1, the proteins with the TagBFP-like chromophore are present (emission band shape at 400–450 nm) and, in turn, we hypothesize that the increase in the emission intensity of the devices operating under ambient might be ascribed to this process that occurs in parallel with the water assisted Glu 215 deprotonation.

In the final stage, all the samples show a quick exponential deactivation of the emission intensity of the chromophore without showing any further blue shift of the chromophore emission band as well as a slight increase in the τ values, while ϕ values are strongly reduced and I_c/I_{tr} ratio further increases Table 1. Thus, once the deprotonation process of Glu 215 has taken place, the protonated chromophore form can easily lose co-planarity, i.e., reduction of ϕ and/or can evolve to the dark *trans* isomer.

Even though the presence of oxygen seems to be beneficial, the overall device stability (*i.e.*, time to reach half of the initial emission intensity) is lower for devices operating under ambient compared to those in inert, *namely* 40 h (**a-a**) vs. 90 h (**a-i**) and 100 h (**b-a**) vs. 140 h (**b-i**) Figure 1. Since the deprotonation process of the Glu 215 is always present regardless of the operation condition, the oxygen-assisted dye transformation will not imply the formation of native mCherry chromophore rather than a chromophore form that is already prone to lose co-planarity as suggested by the sharp final intensity decay. Thus, stable mCherry-polymer bio-phosphors will require hydrophilic polymers with a high and/or tunable oxygen barrier, high stiffness, low residual water content, and easy water processability. Here, PVA derivatives, which have demonstrated a high compatibility with bio-compounds and/or living organisms in hydrogels, represent the best family meeting the above requirements.[43–46] To the best of our knowledge, FP stabilization in PVA-based thin films/coatings has been poorly studied, focusing on solvent-free cryopreservation purposes.[47–51]

2.2. Preparation and Characterization of mCherry-PVA Bio-Phosphors

Bio-phosphors with Mowiol 18–88, 20–98, and 28–99 were prepared in a dome-like shape (5 mm diameter and 5 mm height – Figure 3) by adding mCherry (1 mg) to a PVA solution in milli-Q water (6% PBS) under gentle stirring condition at room temperature. This was followed by a drying process under vacuum - see Experimental Section. The above selection of PVA derivatives allowed us to carry out a direct comparison with respect to the increase of the hydroxylation grade keeping the molecular weight, i.e., Mw ≈125000–145,00, increasing the hydroxylation going from 88% to 98% and 99%;
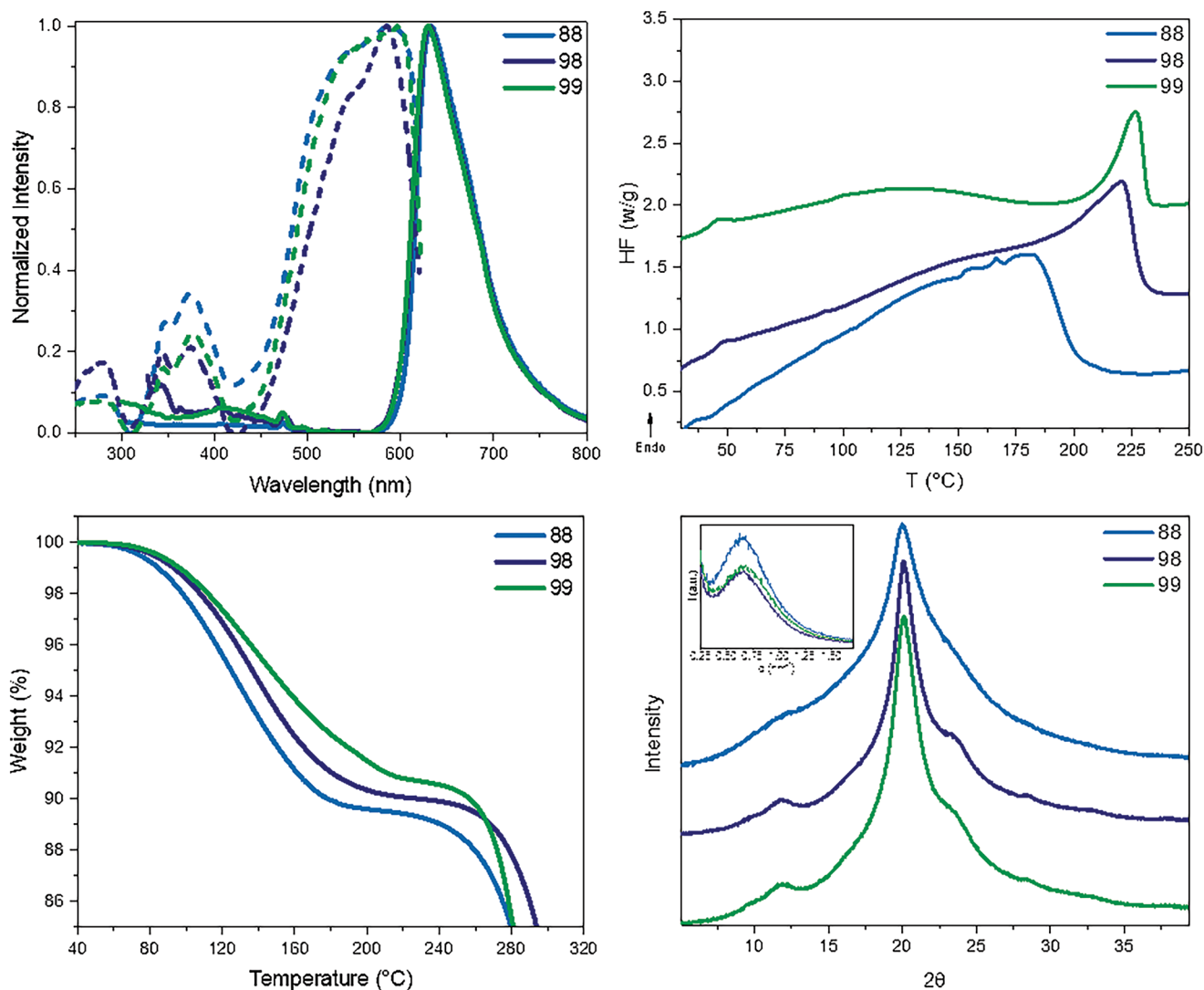
Figure 2. Characterization of **mCherry-PVA-88/98/99** bio-phosphors - see legend. Top, left: Emission (solid line; $\lambda_{exc} = 280$ nm) and excitation (dashed line; $\lambda_{em} = 680$ nm) spectra. Top, right: DSC thermograms. Bottom, left: TGA assays under ambient. Bottom, right: SAXS/WAXS analysis.

mCherry-PVA-88/98/99, respectively. This goes hand-in-hand with the crystallinity degree that rules the amount of trapped water and the permeability to oxygen – vide infra.

Likewise, the reference mCherry-based bio-phosphors Section 2.1, the emission and excitation spectra of all the mCherry-PVA-based coatings consist of i) a broad and intense emission band centered at 630 nm (maturated chromophore) along with a broad and very weak emission band centered at 420 nm (TagBFP-like form of the chromophore) and ii) three broad excitation bands centered at 590 and 390 nm (chromophore) and 280 nm (Tryptophan amino acid), suggesting a similar degree of agglomeration to that of the reference coatings – **Figures** 1 and **2**. What is more relevant, the photoluminescence figures, i.e., τ of *ca.* 1.4 ns and ϕ *ca.* 20% – **Table 2**, confirm that the mCherry is successfully stabilized in this novel matrix upon preparation of coatings regardless of the hydroxylation degree.

Concerning the thermal and structural features of **mCherry-PVA-88/98/99**, they were studied by combining

i) thermogravimetric analysis (TGA), ii) differential scanning calorimetry (DSC), and iii) small-angle and wide-angle X-ray scattering techniques (SAXS/WAXS). At first, it is well-known that PVA films retain more water and oxygen upon reducing the crystallinity grade that strongly depends on the content of acetate groups.[52] In this line, TGA results – Figure 2, showed i) a water loss at 100 °C of 2% for mCherry-PVA-88 coatings and 1% for **mCherry-PVA-98** and **mCherry-PVA-99** coatings and ii) a water loss at 160 °C going from 9% (**mCherry-PVA-88**) to 8% (**mCherry-PVA-98**) and 6% (**mCherry-PVA-99**). The effect of the water content is also reflected in the DSC analysis. Here, three thermal transitions were identified in the first heating cycle: i) a large range of temperature for the glass transition (T_g) at ≈40–70 °C due to the plasticizer effect of water molecules, ii) broad endothermic peak in the range 90–170 °C due to evaporation of trapped water molecules; the area of the peak corroborated the TGA results being more intense with the lower deacetylation grade, and iii) melting of the polymeric crystalline phase

**ADVANCED
SCIENCE NEWS**

www.advancedsciencenews.com

**ADVANCED
FUNCTIONAL
MATERIALS**

www.afm-journal.de

Table 2. Photophysical features of fresh/irradiated mCherry-PVA-88/98/99 bio-phosphors.

	λ_{exc} [nm]	λ_{em} [nm]	ϕ [%]	τ [ns]	k_r[a)] [s^{-1}]	k_{nr}[b)] [s^{-1}]	I_c/I_{tr}
88 fresh	590	630	20.4	1.53	1.33	5.20	/
88 100 h	590	630	20.1	1.41	1.43	5.67	/
88 2000 h	585	620	12.9	1.36	0.95	6.40	1
98 fresh	585	630	18.5	1.20	1.54	6.79	/
98 100 h	585	630	17.0	1.23	1.38	6.75	/
98 2000 h	585	625	13.8	1.21	1.14	7.12	0.5
99 fresh	590	630	15.7	1.30	1.21	6.48	/
99 100 h	585	630	15.7	1.15	1.37	7.33	/
99 2000 h	585	625	11.7	1.22	0.96	7.24	5

a,b)$\times 10^8$.

showed a clear dependency on hydroxylation degree going from 181 °C (**mCherry-PVA-88**) to 220 °C (**mCherry-PVA-98**) to 227 °C (**mCherry-PVA-99**) close to the reported at *ca.* 230 °C for highly deacetylated PVA.[52] This higher melting temperature is related to the size and the perfection of the crystalline region, which is favored if the defect content in the polymer chains (acetate groups) is low.

Finally, these findings were further confirmed by X-ray scattering techniques. While all the coatings feature a similar WAXS pattern with a main peak centered at 20° that corresponds to the $10\overline{1}$ and 101 reflections of a monoclinic unit cell,[53] the hydroxylation degree affected the width and area of the crystalline diffraction – Figure 2. In detail, **mCherry-PVA-99** exhibited the narrowest and highest reflection, corroborating that the lowest number of defects favor the formation of large crystalline domains. **mCherry-PVA-98** and **mCherry-PVA-88** featured a progressive broadening and intensity reduction, suggesting that the amorphous domain increases as noted by DSC – Figure 2. Finally, SAXS results showed a similar broad peak centered at q ≈0.65 nm^{-1}. This reflection is related to long spacing, which is the average length of the crystalline lamella plus amorphous region. Therefore, the crystal morphology of the coatings is similar for all coatings, that is, organized in crystal lamella separated by amorphous regions with a sequential length of ≈10 nm, and a reduction of the crystalline domain amount with the acetylation grade. Thus, we can conclude that **mCherry-PVA-99** with the highest hydroxylation degree features larger crystallinity domains leading to lower trapped water content as well as the best oxygen barrier.

2.3. Preparation and Characterization of mCherry-PVA Bio-HLEDs

Deep-red Bio-HLEDs were prepared by combining **mCherry-PVA-88/98/99** coatings with a 590 nm LED chip using an on-chip configuration and measuring under ambient conditions as explained in Section 2.1. Regardless of the bio-phosphor configuration, all the devices showed a full conversion of the LED emission at the applied current range of 10–200 mA – **Figure 3**. The device chromaticity corresponds to the deep-red region associated with a broad emission band centered at 650 nm x/y CIE color coordinates of 0.61/0.32 and external quantum efficiency (EQE) values of ≈0.4% (radian flux of 1050 µW at 200 mA) – Figure 3. The moderate efficiencies of our coatings should be ascribed to i) scattering events at both the surface and inside the coating, and ii) reabsorption events due to the limited Stokes Shift of mCherry. Both these aspects are not negligible in a 5 mm thick coating - see Section 2.2. In addition, we ascribe the slight differences between the EQEs of the **mCherry-PVA-88/98/99** coatings to scattering phenomena which could depend on the distribution and size of the crystalline domains.

Figures 4 and **5** display the device stability using high-power excitation flux (200 mA, 55 mW cm^{-2}) under ambient conditions. Likewise, in reference to mCherry-TMPE:PEO devices, the temperature of the coatings was held constant (< 30°C). However, the emission intensity changes do not show any recovery process related to the influence of oxygen, as expected by the higher stiffness and oxygen barrier features compared to TMPE:PEO coatings - vide infra. What is more, the PVA devices clearly outperformed the best reference device (50/140 h ambient/inert – Figure 1), reaching a remarkably enhanced device lifetime going from 1,100 to 2,000 h, and to 2,600 h for **mCherry-PVA-88/98/99** devices, respectively. In short, a first intensity decay reaching a 300 h plateau was related to an average intensity loss of *ca.* 10% (**mCherry-PVA-99**) and 20% (**mCherry-PVA-88** and **-98**) in concert with i) a 10 nm blue-shifted emission of the chromophore – Figure 5, ii) a reduction of τ without affecting ϕ– Table 2, and iii) a non-meaningful impact on the I_c/I_{tr} values – Table 2 and Figure 5. Thus, this first step is attributed to the combination of the photo-induced isomerization and the slow deprotonation of the Glu 215 amino acid. The latter deactivation process is ongoing over the following 1200–1,700 h – Figure 5 and Table 2, showing a further intensity loss of 20%, 10%, and 0% for **mCherry-PVA-88/98/99** devices, respectively. This difference might be related to the amount of trapped water in the coatings – Figure 2, as this deactivation mechanism is related to the H-transfer from the Glu 215 to the imidazolinone moiety of the chromophore.[54] Indeed, once this process is over, *i.e.*, no more blue shift of the maximum emission wavelength, all the devices showed a drastic decay of the emission intensity associated to a reduction of the ϕ values - Table 2, indicating a loss of the
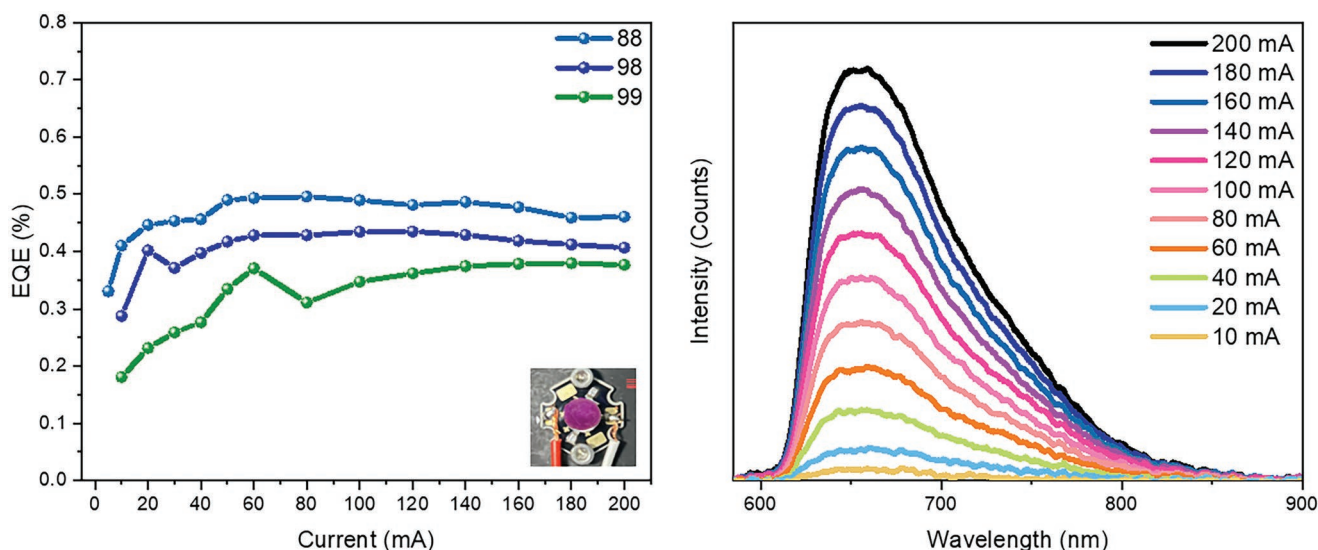
Figure 3. Characterization of **mCherry-PVA-88/98/99** Bio-HLEDs. Left: Average EQE values upon increasing the applied current; Inset: **mCherry-PVA-99** phosphor placed on top of the 590 nm pumping chip. Right: Emission spectra of **mCherry-PVA-99** Bio-HLED upon increasing the applied current see legend.

co-planarity of the chromophore structure and/or a quick transformation to the *trans* form as noted in reference bio-phosphors - Section 2.1.[55]

3. Conclusion

To date, red-emitting Bio-HLEDs based on the archetypal mCherry have been limited by their poor stability, i.e., < 50 and < 140 h under ambient and inert conditions, respectively. This is key to develop *i)* highly performing white-emitting Bio-HLEDs for general illumination purposes, as green Bio-HLEDs have reached stabilities of ca. 3,500 h,[7,16] as well as *ii)* low-energy

Figure 4. Intensity decay ($\lambda_{em} = 680$ nm) of **mCherry-PVA-88/98/99** Bio-HLEDs driven at 200 mA (55 mW cm^{-2}) with on chip configuration under ambient conditions. The three phosphors irradiated upon the aforementioned conditions showed constant temperature < 30 °C.

emitting single-point sources of high interest for phototherapy, communications, vertical farming, *etc.*[7] Based on a comprehensive study merging photophysical/thermal/structural features as well as device degradation (ambient/inert) using reference polymer composite prepared with H_2O and D_2O, we have identified that the deactivation mechanism of mCherry strongly depends on the operating atmosphere. Under inert conditions, this consists of an initial photo-induced *cis–trans* isomerization of the ionic form of the chromophore that reduces the emission intensity, followed by a progressive H-transfer from Glu 215 to imidazolinone moiety of the chromophore leading to a protonated conformation. The latter quickly becomes non-emissive losing its co-planar conformation or further evolving to its *trans* configuration. In contrast, ambient operation promotes an additional oxygen-driven transformation of the TagBFP-like chromophore (non-maturated mCherry) to its native emissive form. While this could be thought of as beneficial, the overall device stability is even less than half upon comparing ambient versus inert conditions. Hence, we explored hydrophilic polyvinyl alcohol derivatives, producing FP-PVA bio-phosphors, in which the emission features of mCherry are preserved and the amount of trapped water and crystallinity (oxygen/moisture barrier) is controlled via the hydroxylation degree.[52,56,57] While the latter prevented the oxidation process in devices operating under ambient conditions, the amount of trapped water was instrumental to slow down the H-transfer deactivation process of the chromophore. This led to remarkably enhanced device lifetimes of 1,100 to 2,000, and 2,600 h for **mCherry-PVA-88/98/99**, respectively.

What is paramount, devices with **mCherry-PVA-99** bio-phosphor exhibited first-class stability compared to the prior art with a brightness loss of < 5% over 3.5 months which is alike to the best green-emitting Bio-HLED to date.[16] Still, the device efficiency is moderate, but it can be increased by i) reducing the thickness of the coatings to avoid scattering loss processes, ii) micro-structuration of the coating surface to increase light
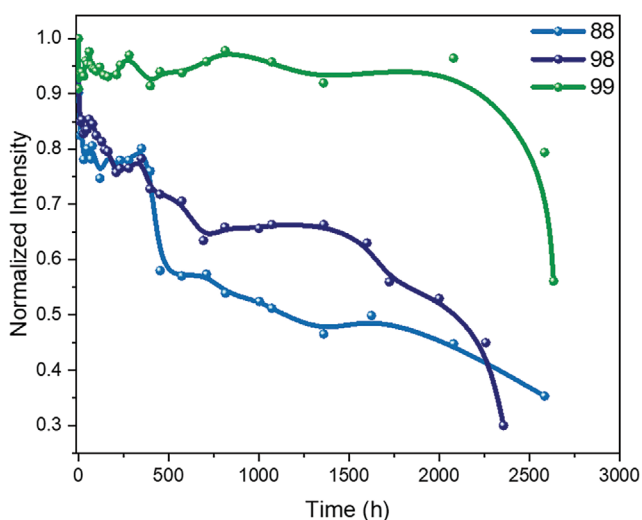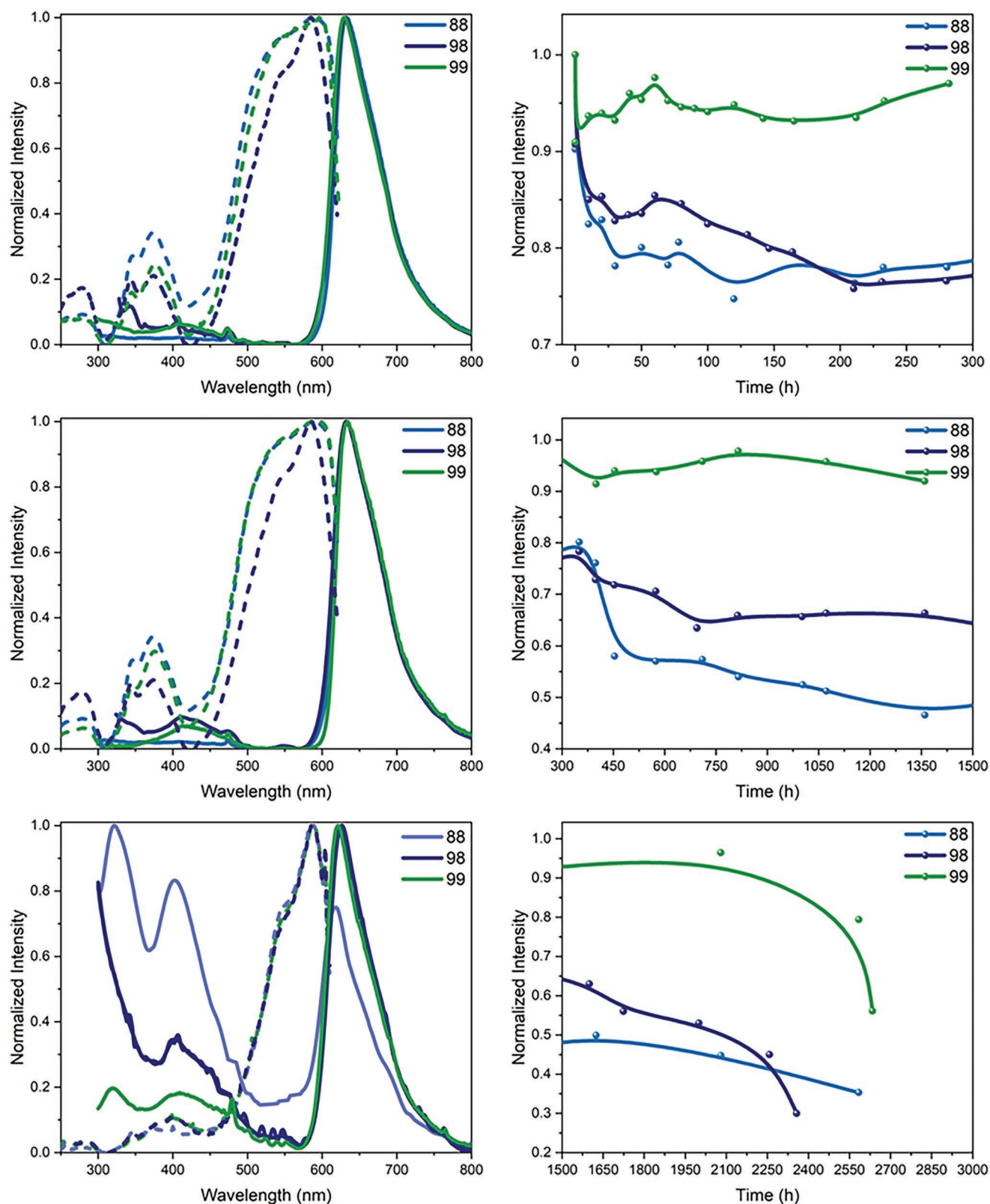
Figure 5. Emission (solid line; λ_{exc} = 280 nm) and excitation (dashed line; λ_{em} = 680 nm) spectra (left) of the **mCherry-PVA-88/98/99** bio-phosphors at each Bio-HLED degradation stage (right; top: 0–300 h, center: 300–1500 h; bottom: 1500–3000) when driven at 200 mA (55 mW cm^{-2}) with on chip configuration under ambient conditions. The three phosphors irradiated upon the aforementioned conditions showed constant temperature <30 °C.

out-coupling, as well as *iii*) redesigning mCherry to improve its stokes shift and ϕ.

Overall, this work sets in a comprehensive rationale for to search for homopolymer matrices in bio-phosphors designed for lighting purposes, overpassing the frontier stability limit of deep-red-emitting Bio-HLEDs toward meeting the milestone of highly stable white-emitting Bio-HLEDs in near future.

4. Experimental Section

Protein Production and Purification: mCherry was expressed in *Escherichia coli* BL21 and purified by Ni-NTA affinity chromatography, followed by gel filtration on a HiLoad 26/600 Superdex 75pg column in phosphate buffer saline (PBS) buffer. Purified proteins were frozen immediately in liquid nitrogen and stored at -80 °C. Thawed proteins were centrifuged at 14 000 rpm for 30 min at 4 °C, and the supernatant was used for the measurements.

Preparation and Characterization of Bio-Phosphors: The bio-phosphors were prepared by adding a solution of mCherry (1 mg) to a solution of Mowiol. The samples were dried overnight in a vacuum chamber at 1 mbar. The reference rubber-like coatings **a** and **b** were prepared with a mass ratio 4:1 (TMPE:PEO). A mQ water (a) or D_2O (b) solution (6% PBS) bearing 1 mg of mCherry was added to TMPE and stirred together with PEO. The samples were dried overnight in a vacuum chamber at 3 mbar, following reported procedures.[9] The photophysical characterization (excitation and emission spectra, ϕ, τ) was carried out with an FS5 Spectrofluorometer from Edinburgh Instruments, using an SC-5 module for liquid samples, SC-10 module for solid samples, and SC-30 Integrating Sphere to determine ϕ (λ_{exc} = 530 nm). All measurements were performed at RT in ambient.

Preparation and Characterization of the Coatings: All reagents were purchased from Sigma-Aldrich, specifically: Mowiol 18–88 M_w ≈130 000, Mowiol 20–98 M_w ≈125 000, Mowiol 28–99 M_w ≈145 000. The coatings for the mechanical tests were prepared by dissolution of Mowiol under gentle stirring conditions on a hot plate. The samples were then dried overnight under vacuum conditions after addition of a PBS aliquot at RT. The differential scanning calorimetry was performed with a Q200 DSC from TA Instruments with a rate of 10 °C min⁻¹. The thermal gravimetric analysis was performed with TGA-Q50 from TA instruments analyzer under an N_2 atmosphere with a heating rate of 10 °C min⁻¹. SAXS/WAXS experiments were performed in an Anton Paar SAXSpoint 5.0, equipped a primux 100 micro microfocus using Cu as target and a 2D HPC Detector (EIGER2 R 1 M). The distance between sample and detector was 100 and 800 mm for WAXS and SAXS respectively. The analysis of the data was performed in Anton Paar SAXS analysis software.

Device Fabrication and Characterization: The devices were fabricated using 590 nm LED chips (WINGER WEPYE1-S1 Power LED Star) as pumping sources. To carry out the photostability and conversion measurements the bio-phosphors were placed in on-chip configuration and driven either at different currents to study conversion and efficiency or at 200 mA (55 mW cm⁻²) for long-term stability at ambient and inert N_2 atmosphere (0.1 ppm O_2, < 0.05 ppm H_2O). The electroluminescence spectra were recorded through Avantes Spectrometer 2048L (300 VA grating, 200 μm slit, CCD detector) coupled with an AvaSphere 30-Irrad Integrated sphere, monitoring the temperature using a thermographic camera FLIR ETS320. The employed power source was a Keithley 2231-A-30-3.

Supporting Information

Supporting Information is available from the Wiley Online Library or from the author.

Conflict of Interest

The authors declare no conflict of interest.

Data Availability Statement

The data that support the findings of this study are available from the corresponding author upon reasonable request.

Keywords

[1] M. H. Fang, Z. Bao, W. T. Huang, R. S. Liu, *Chem. Rev.* **2022**, *122*, 11474.

[2] E. Fresta, V. Fernández-Luna, P. B. Coto, R. D. Costa, *Adv. Funct. Mater.* **2018**, *28*, 1707011.

[3] G. B. Nair, H. C. Swart, S. J. Dhoble, *Prog. Mater. Sci.* **2020**, *109*, 100622.

[4] P. Gaffuri, E. Stolyarova, D. Llerena, E. Appert, M. Consonni, S. Robin, V. Consonni, *Renewable Sustainable Energy Rev.* **2021**, *143*, 110869.

[5] S. Wahl, M. Engelhardt, P. Schaupp, C. Lappe, I. V. Ivanov, *J. Biophotonics* **2019**, *12*, 201900102.

[6] G. Salviulo, M. Lavagnolo, M. Abalà, E. Bernardo, A. Polimeno, M. Sambi, F. Bonollo, S. Gross, *Chem. - Eur. J.* **2021**, *27*, 6676.

[7] M. Pattinson, M. Hansen, N. Bardsley, G. Thomson, K. Gordon, A. Wilkerson, K. Lee, V. Nubbe, S. Donnelly, *DOE BTO Solid-State Lighting Program, "2022 DOE SSL R&D Opportunities,"*, US Department of Energy, Washington, DC **2022**.

[8] *Hybrid Phosphor Materials*, (Eds.: K. Upadhyay, S. Thomas, R. Tamraka), Springer, Cham **2022**.

[9] L. Niklaus, H. Dakhil, M. Kostrzewa, P. B. Coto, U. Sonnewald, A. Wierschem, R. D. Costa, *Mater. Horiz.* **2016**, *3*, 340.

[10] J. He, S. Yang, K. Zheng, Y. Zhang, J. Song, J. Qu, *Green Chem.* **2018**, *20*, 3557.

[11] H. Guo, Z. Liu, X. Shen, L. Wang, *ACS Sustainable Chem. Eng.* **2022**, *10*, 8289.

[12] B. Liu, H.-Y. Duan, Y.-L. Wang, B.-Y. Du, Q. Yang, J.-T. Xu, Y.-Z. Yang, A. Greiner, X.-H. Zhang, *Mater. Horiz.* **2018**, *5*, 932.

[13] P. Schlotter, R. Schmidt, J. Schneider, *Appl. Phys. A* **1997**, *64*, 417.

[14] F. Hide, P. Kozodoy, S. P. DenBaars, A. J. Heeger, *Appl. Phys. Lett.* **1997**, *70*, 2664.

[15] M. D. Weber, L. Niklaus, M. Pröschel, P. B. Coto, U. Sonnewald, R. D. Costa, *Adv. Mater.* **2015**, *27*, 5493.

[16] A. Espasa, M. Lang, C. F. Aguiño, D. Sanchez-deAlcazar, J. P. Fernández-Blázquez, U. Sonnewald, A. L. Cortajarena, P. B. Coto, R. D. Costa, *Nat. Commun.* **2020**, *11*, 879.

[17] M. S. P. Reddy, C. Park, *Sci. Rep.* **2016**, *6*, 32306.

[18] K. Benson, A. Ghimire, A. Pattammattel, C. V. Kumar, *Adv. Funct. Mater.* **2017**, *27*, 1702955.

[19] D. Zhou, H. Zou, M. Liu, K. Zhang, Y. Sheng, J. Cui, H. Zhang, B. Yang, *ACS Appl. Mater. Interface* **2015**, *7*, 15830.

[20] M. Sun, S. Qu, Z. Hao, W. Ji, P. Jing, H. Zhang, L. Zhang, J. Zhao, D. Shen, *Nanoscale* **2014**, *6*, 13076.

[21] H. Tetsuka, A. Nagoya, R. Asahi, *J. Mater. Chem. C* **2015**, *3*, 3536.

[22] V. Fernández-Luna, D. Sánchez-de Alcázar, J. P. Fernández-Blázquez, A. L. Cortajarena, P. B. Coto, R. D. Costa, *Adv. Funct. Mater.* **2019**, *29*, 1904356.

[23] L. Niklaus, S. Tansaz, H. Dakhil, K. T. Weber, M. Pröschel, M. Lang, M. Kostrzewa, P. B. Coto, R. Detsch, U. Sonnewald, A. Wierschem, A. R. Boccaccini, R. D. Costa, *Adv. Funct. Mater.* **2017**, *27*, 1601792.

[24] C. F. Aguino, M. Lang, V. Fernández-Luna, M. Pröschel, U. Sonnewald, P. B. Coto, R. D. Costa, *ACS Omega* **2018**, *3*, 15829.

[25] X. Wang, Y. Guo, Z. Li, W. Ying, D. Chen, Z. Deng, X. Peng, *RSC Adv.* **2019**, *9*, 9777.

[26] X. Wang, Z. Li, W. Ying, D. Chen, P. Li, Z. Deng, X. Peng, *J. Mater. Chem. C* **2019**, *8*, 240.

[27] A. Aires, V. Fernández-Luna, J. Fernandez-Cestau, R. D. Costa, A. L. Cortajarena, *Nano Lett.* **2020**, *20*, 2710.

[28] S. Ferrara, S. H. Mejias, M. Liutkus, G. Renno, F. Stella, I. Kociolek, J. P. Fuenzalida-Werner, C. Barolo, P. B. Coto, A. L. Cortajarena, R. D. Costa, *Adv. Funct. Mater.* **2022**, *32*, 2111381.

[29] V. Fernández-Luna, J. P. Fernández-Blázquez, M. A. Monclús, F. J. Rojo, R. Daza, D. Sanchez-Dealcazar, A. L. Cortajarena, R. D. Costa, *Mater. Horiz.* **2020**, *7*, 1790.

[30] S. Sadeghi, R. Melikov, D. Conkar, E. N. Firat-Karalar, S. Nizamoglu, *Adv. Mater. Technol.* **2020**, *5*, 2070035.

[31] X. Shu, N. C. Shaner, C. A. Yarbrough, R. Y. Tsien, S. J. Remington, *Biochemistry* **2006**, *45*, 9639.

[32] T. J. Lambert, *Nat. Methods* **2019**, *16*, 277.

[33] F. V. Subach, V. V. Verkhusha, *Chem. Rev.* **2012**, *112*, 4308.

[34] J. L. Tubbs, J. A. Tainer, E. D. Getzoff, *Biochemistry* **2005**, *44*, 9833.

[35] K. Mishra, J. P. Fuenzalida-Werner, F. Pennacchietti, R. Janowski, A. Chmyrov, Y. Huang, C. Zakian, U. Klemm, I. Testa, D. Niessing, V. Ntziachristos, A. C. Stiel, *Nat. Biotechnol.* **2021**, *40*, 598.

[36] S. Legault, D. P. Fraser-Halberg, R. L. McAnelly, M. G. Eason, M. C. Thompson, R. A. Chica, *Chem. Sci.* **2022**, *13*, 1408.

[37] A. T. Pandelieva, M. J. Baran, G. F. Calderini, J. L. McCann, V. Tremblay, S. Sarvan, J. A. Davey, J. F. Couture, R. A. Chica, *ACS Chem. Biol.* **2016**, *11*, 508.

[38] J. P. Fuenzalida Werner, Y. Huang, K. Mishra, R. Janowski, P. Vetschera, C. Heichler, A. Chmyrov, C. Neufert, D. Niessing, V. Ntziachristos, A. C. Stiel, *Anal. Chem.* **2020**, *92*, 10717.

[39] J. C. Prangsma, R. Molenaar, L. Van Weeren, D. S. Bindels, L. Haarbosch, J. Stouthamer, T. W. J. Gadella, V. Subramaniam, W. L. Vos, C. Blum, *J. Phys. Chem. B* **2020**, *124*, 1383.

[40] W. Q. Ong, Y. R. Citron, J. Schnitzbauer, D. Kamiyama, B. Huang, *Chem. Commun.* **2015**, *51*, 13451.

[41] F. V. Subach, G. H. Patterson, S. Manley, J. M. Gillette, J. Lippincott-Schwartz, V. V. Verkhusha, *Nat. Methods* **2009**, *6*, 153.

[42] O. V. Stepanenko, O. V. Stepanenko, D. M. Shcherbakova, I. M. Kuznetsova, K. K. Turoverov, V. V. Verkhusha, *BioTechniques* **2011**, *51*, 313.

[43] Y. Wen, F. Wei, W. Xu, X. Jiang, J. Cui, Y. Ai, J. Chen, A. Cui, Z. Hu, J. Fu, S. Liu, Q. He, J. Cheng, *Chem. Commun.* **2020**, *56*, 3191.

[44] D. A. Bichara, X. Zhao, H. Bodugoz-Senturk, F. P. Ballyns, E. Oral, M. A. Randolph, L. J. Bonassar, T. J. Gill, O. K. Muratoglu, *Tissue Eng., Part A* **2010**, *17*, 301.

[45] S. Sakai, M. Tsumura, M. Inoue, Y. Koga, K. Fukano, M. Taya, *J. Mater. Chem. B* **2013**, *1*, 5067.

[46] M. Chaouat, C. L.e Visage, W. E. Baille, B. Escoubet, F. Chaubet, M. A. Mateescu, D. Letourneur, *Adv. Funct. Mater.* **2008**, *18*, 2855.

[47] C. Holmström, P. Steinberg, V. Christov, G. Christie, S. Kjelleberg, *Biofouling* **2000**, *15*, 109.

[48] M. Szczsna-Antczak, E. Galas, *Biomol. Eng.* **2001**, *17*, 55.

[49] M. Cotlet, J. Hofkens, F. Köhn, J. Michiels, G. Dirix, M. Van Guyse, J. Vanderleyden, F. C. De Schryver, *Chem. Phys. Lett.* **2001**, *336*, 415.

[50] S. Yoshioka, Y. Aso, Y. Nakai, S. Kojima, *J. Pharm. Sci.* **1998**, *87*, 147.

[51] A. E. R. Fayter, M. Hasan, T. R. Congdon, I. Kontopoulou, M. I. Gibson, *Eur. Polym. J.* **2020**, *140*, 110036.

[52] V. S. Pshezhetskii, A. A. Rakhnyanskaya, I. M. Gaponenko, Y. E. Nalbandyan, *Polym. Sci. USSR* **1990**, *32*, 722.

[53] R. Ricciardi, F. Auriemma, C. De Rosa, F. Lauprêtre, *Macromolecules* **2004**, *37*, 1921.

[54] X. Shu, N. C. Shaner, C. A. Yarbrough, R. Y. Tsien, S. J. Remington, *Biochemistry* **2006**, *45*, 9639.

[55] F. V. Subach, L. Zhang, T. W. J. Gadella, N. G. Gurskaya, K. A. Lukyanov, V. V. Verkhusha, *Chem. Biol.* **2010**, *17*, 745.

[56] C. K. Regmi, Y. R. Bhandari, B. S. Gerstman, P. P. Chapagain, *J. Phys. Chem. B* **2013**, *117*, 2247.

[57] A. Nyflött, C. Meriçer, M. Minelli, E. Moons, L. Järnström, M. Lestelius, M. G. Baschetti, *J. Coatings Technol. Res.* **2017**, *14*, 1345.